Model-Based Reconstruction of Spectral and Spatial Source Distribution from Objects with Known Motion

Jason M. Jaworski *Student Member, IEEE*, Christopher G. Wahl *Student Member, IEEE*, Weiyi Wang *Student Member, IEEE*, Jeffrey A. Fessler *Fellow, IEEE*, and Zhong He, *Senior Member, IEEE*

***Abstract*– A model-based activity reconstruction in both the energy and spatial domains is developed that includes separate parameterization for any objects moving with known motion. This approach corrects for object motion, without smearing the stationary backdrop space. The goal is to simultaneously obtain an energy-dependent spatial map of the radiation field for the backdrop and for each parameterized moving object. Experimental results show that the method can successfully reconstruct the activity of moving objects while also revealing stationary sources in the backdrop. Also, by including the possibility of partial photon energy deposition in the detector in the model, the incident energy spectrum is reconstructed more accurately.**

I. Introduction

In some applications, such as homeland security, the imaging and/or detection of gamma sources in moving objects is desired. In certain situations, there may also be significant sources of gamma radiation in the stationary backdrop. For these scenarios, an algorithm is needed that can correctly reconstruct the radiation originating from the moving objects, as well as the stationary sources without crosstalk between them. With the use of position-sensitive gamma-ray spectrometers [1]-[3] combined with video motion tracking systems [4]-[6], Compton imaging that compensates for the object motion is possible. This capability is combined with the model-based reconstruction presented here to deconvolve the moving-target image and spectrum from those of the backdrop.

II. Model

A. Data Model

Let v denote an attribute vector recorded by a position-sensitive detector such as a Compton-imaging system. For example, if an event interacts twice in a 3D detector, then v may have eight elements: the energies and the 3D positions of the two interactions.

A list-mode acquisition for a fixed scan duration τ_d records M attributes $v_1,\ldots,v_M$ at corresponding times $t_1,\ldots,t_M$. The goal is to reconstruct images from these measurements.

A gamma-ray imaging system is characterized by a system model that consists of some probability distributions that are assumed to be known, *i.e.*, are modeled based on the physics of the system. One component is the system *sensitivity* function:

$$s(\vec{r},E)=\mathsf{p}(D;\vec{r},E),$$

which describes the probability that a gamma-ray emission from spatial position $\vec{r}$ at energy E is detected (D) by the system. For a single detector often $\vec{r}$ denotes coordinates on a sphere, *i.e.*, the far field; whereas for a system with multiple detectors it is reasonable to consider 3D image reconstruction where $\vec{r}\in\Re^3$. This work focuses on the case of a single detector system where the 2D coordinates on a sphere are used.

Another model component that is needed is

$$\mathsf{p}(v\mid D;\vec{r},E)$$

which describes the distribution of recorded attributes v for emissions originating from spatial position $\vec{r}$ and energy E. A system may also record attributes from background sources that are not part of the scene being modeled; the distribution of such attributes is denoted

$$\mathsf{p}(v\mid D;B).$$

It is assumed that this distribution is known, *e.g.*, through calibration. Sometimes it is assumed to be zero. The rate λ_b at which such background events are recorded might be known or unknown.

B. Target Object Model

For a static (stationary) scene, the usual goal is to reconstruct the spatial (radio)activity distribution $\lambda(\vec{r},E)$ from the measured list-mode data, and the existing list-mode approach [7]-[9] is appropriate. This work extends this formulation to the case where the scene consists of one or more target objects that are moving relative to a stationary backdrop, *i.e.*, the overall activity distribution is a function of time: $\lambda(\vec{r},E,t)$. We consider here the case of "known" motion, *i.e.*, the motion is estimated separately, for example by a video tracking system.

The activity distribution is modeled as consisting of a stationary backdrop having unknown activity distribution $\lambda_0(\vec{r},E)$ and a set of K target objects that may be moving. The unknown activity distribution of the kth object at time t = 0 is denoted

$$\lambda_k(\vec{r},E)\equiv\lambda_k(\vec{r},E,0).$$

Manuscript received November 21, 2010. This work was supported in part by the U.S. Department of Homeland Security under Grant No. BS123456 .

The authors are with the Nuclear Engineering and Radiological Sciences Department, and the Electrical Engineering and Computer Science Department, University of Michigan, Ann Arbor, MI 48109-2122 USA (e-mail: jasonjaw@umich.edu)

For simplicity of presentation, it is assumed the target object motion can be modeled adequately by a spatial translation. Other forms of motion, such as rotation, could be accommodated as well. The spatial shift of the *k*th target object at time *t* is denoted $\vec{c}_k(t)$, where $\vec{c} \in \Re^3$ for a 3D imaging problem. Under this assumption, the activity distribution of the *k*th target object at time *t* is given by

$$\lambda_k(\vec{r}, E, t) = \lambda_k(\vec{r} - \vec{c}_k(t), E).$$

For simplicity, occlusions and the absorption of gamma photons by target objects that move in front of one another are ignored. Then the overall time-varying activity distribution of the scene as the superposition of the stationary backdrop and the moving target object contributions is modeled as:

$$\begin{aligned} \lambda(\vec{r}, E, t) &= \lambda_0(\vec{r}, E) + \sum_{k=1}^{K} \lambda_k(\vec{r}, E, t) \\ &= \lambda_0(\vec{r}, E) + \sum_{k=1}^{K} \lambda_k(\vec{r} - \vec{c}_k(t), E). \end{aligned} \quad (1)$$

The goal is to reconstruct the activity distributions of the backdrop and the target objects, *i.e.*, $\{\lambda_0(\vec{r}, E), \lambda_1(\vec{r}, E), \ldots, \lambda_K(\vec{r}, E)\}$, from the list-mode data, assuming known motion $\vec{c}_k(t)$.

To facilitate numerical implementation, the activity distributions are parameterized using a finite-series model [10]:

$$\lambda_0(\vec{r}, E) = \sum_{j=1}^{N} \lambda_{0j} b_{0j}(\vec{r}, E), \quad (2)$$

where λ_{0j} denotes the unknown activity of the *j*th basis function and b_{0j} denotes the basis function (typically a 2D region of space in the spherical coordinates or a voxel in the 3D coordinates, at a certain energy). Similarly the moving target objects are parameterized (at time *t*=0) as:

$$\lambda_k(\vec{r}, E) = \sum_{j=1}^{N_k} \lambda_{kj} b_{kj}(\vec{r}, E), \quad (3)$$

where the number of basis functions N_k used to represent the *k*th target object may differ between target objects of different sizes. If the *k*th moving target object is treated as a point source, then N_k is the number of energy bins. The overall time-varying activity distribution is thus parameterized as:

$$\lambda(\vec{r}, E, t) = \sum_{j=1}^{N} \lambda_{0j} b_{0j}(\vec{r}, E) + \sum_{k=1}^{K} \sum_{j=1}^{N_k} \lambda_{kj} b_{kj}(\vec{r} - \vec{c}_k(t), E).$$

Typically, the basis functions are unitless and the coefficients λ_{kj} have units "emissions per second per unit volume per unit energy."

With this parameterization, the goal is to estimate the coefficients $\{\lambda_{0j}\}$ and $\{\lambda_{kj}, k = 1, \ldots, K\}$ from the list-mode data. Fig. 1 illustrates the model. Note that if the *k*th target object does not move, then this formulation could be over-parameterized because the activity within the support of that target object could be modeled both by the target object pixel λ_{kj} and a corresponding backdrop pixel $\lambda_{0j'}$, in the case that $b_{j'}(\vec{r})$ and $b_{kj}(\vec{r})$ overlap. So one should include only moving target objects in this formulation otherwise there can be no unique solution.

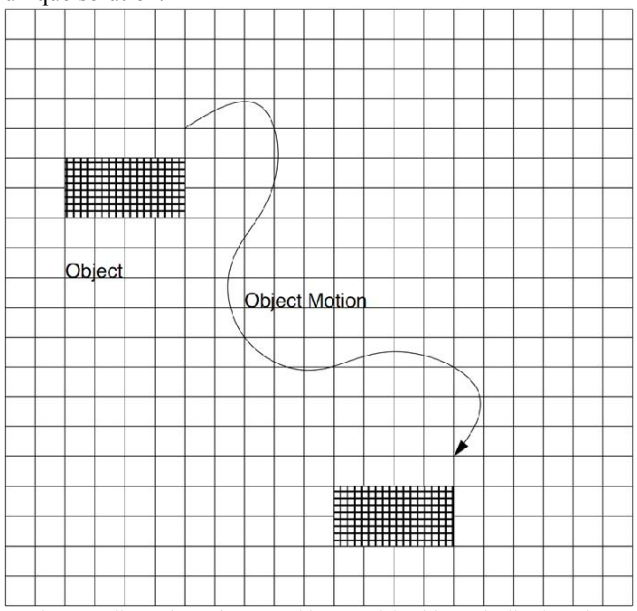

Fig. 1. Illustration of target object model with a pixelized stationary backdrop and one pixelized target object that moves around during the imaging process.

III. Algorithm

One can show that the general form of the list-mode log-likelihood for a time-varying emission distribution $\lambda(\vec{r}, E, t)$ is

$$\sum_{m=1}^{M} \log\left(\iint \mathsf{p}(v_m \mid D; \vec{r}, E) \lambda(\vec{r}, E, t_m) d\vec{r} dE + \mathsf{p}(v_m \mid D, B) \lambda_b(t_m) \right) - \mathsf{E}[M]$$

where the expected number of recorded counts is given by

$$\mathsf{E}[M] = \int_0^{\tau_d} \lambda_s(t) + \lambda_b(t) dt$$

$$\lambda_s(t) \equiv \iint s(\vec{r}, E) \lambda(\vec{r}, E, t) d\vec{r} dE,$$

where $\lambda_b(t)$ denotes the counting rate due to background events.

Substituting in the finite-series models (1) and (3) yields a log-likelihood expression in terms of the coefficients $\{\lambda_{0j}\}$ and $\{\lambda_{kj}\}$.

A pixel grid similar to that of the backdrop (with fewer elements and covering a smaller region) is used to spatially parameterize each of the moving target objects. The physical direction that corresponds to the target object grid pixels is defined by $\vec{c}_k(t)$, but the target object grid can be considered as extra pixels in an extension of the backdrop grid, and the standard list-mode EM algorithm for static target objects [9] can be used.

In this work, the model for the “backdrop” is assumed to be sufficient to allow the "background" distribution to be zero, simplifying the implementation.

IV. Experiments

A. Polaris System

The Polaris detector system recorded the data used in this work. This system consists of 18 2.0 cm × 2.0 cm × 1.5 cm pixellated CdZnTe detectors. The array operates as a single detector, *i.e.*, if a photon scatters from one detector into another, the system reads that as one event and is able to use it for Compton imaging. The system is able to achieve 1.08% single-pixel and 1.44% overall FWHM energy resolution at 662 keV. The energy and 3D positions of each interaction for each event (incident photon) are recorded in list mode. These list-mode data for 2-, 3- and 4-interaction events are used for the image reconstruction.

B. Source Motion

Sources with known motion as a function of time are required for the presented algorithm. Thus, an apparatus was assembled to rotate a source around the Polaris array with known motion. Fig. 2 shows a picture of the setup. A computer controlled actuator, attached to the top of a table, was set to rotate with a constant angular velocity to known angular displacements. An 'L'-shaped aluminum arm was attached to this actuator so that the bottom-most tip of the arm was in the plane of the Polaris system positioned below the table. The center of the detector head was placed directly below the actuator pivot point so that the resulting motion at the bottom most tip of the actuator arm would revolve completely around the center of the detector array.

Fig. 2. A computer controlled actuator arm is used to control the position of the source with known motion. The Polaris system is positioned directly underneath the actuator pivot point, and the source is placed at the bottom of the actuator arm in-plane with the detector system.

V. Results

A. One Moving Source

In the first experiment, a ^{137}Cs source was rotated 360° around the detector system in the counterclockwise direction (when viewed from the top). This dataset was reconstructed using a 32 × 64 pixel backdrop mesh (over 4π) and a 9 × 9 pixel target object mesh spanning 20° in the polar and azimuthal directions. 150 evenly spaced energy bins were used over a range of 250 - 850 keV. Very few imagable events fall outside this energy range, so the energy dimension could be limited to this range. Fig. 3 shows the simple back-projection reconstruction for this dataset (number of events used for the reconstruction is shown on the image).

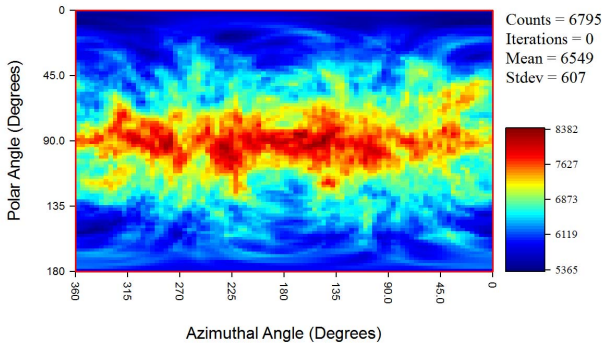

Fig. 3. The uncompensated simple back-projection reconstruction for a single ^{137}Cs source moving 360° around the azimuthal direction.

Even though a point source was used, the reconstruction shows what appears to be a line source along the equator due to the source motion.

Figs. 4 and 5 show the results after 20 EM iterations using the model based algorithm presented in Section III. The expected results would estimate a very low intensity in the backdrop space (due to natural background) and a sharp hotspot at 662 keV in the target object space that tracked the source motion. Fig. 4 shows that the actual reconstructed intensity distribution in the backdrop space is mostly flat, as expected, but the spectrum does show some minor ^{137}Cs contamination at 662 keV. Fig. 5 shows that the estimated intensity for the target object space matches expectations very well. One sharp hotspot at the center of the image space is present with a clean 662 keV photopeak in the spectrum.

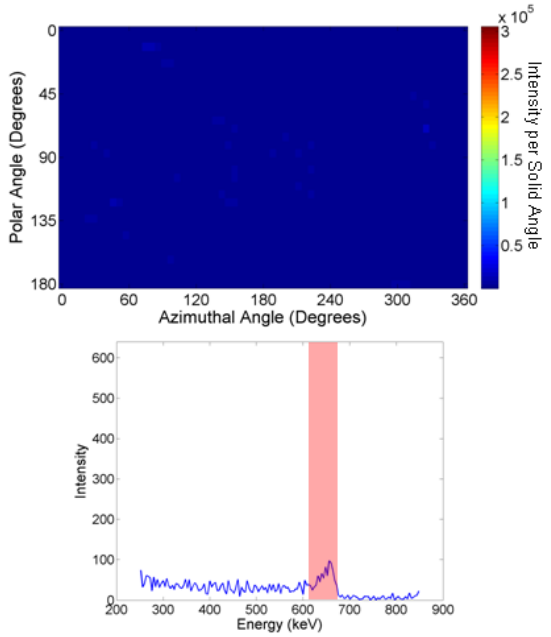

Fig. 4. Results for the backdrop space after 20 EM iterations for a single moving ^{137}Cs source. The upper plot is the deconvolved image for the highlighted ^{137}Cs photopeak, and the lower plot is the deconvolved energy spectrum for the entire backdrop space.

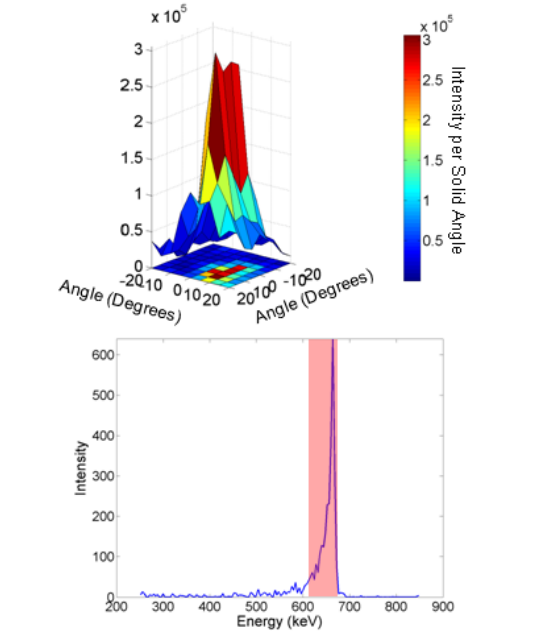

Fig. 5. Results for the target object space after 20 EM iterations for a single moving ^{137}Cs source. The upper plot is the deconvolved image for the highlighted ^{137}Cs photopeak, and the lower plot is the deconvolved energy spectrum for this target.

B. One moving and one stationary source

In the second experiment, a ^{137}Cs source was rotated 360° around the detector system similar to the previous experiment, and a ^{22}Na source was placed in a stationary position in the backdrop. This dataset was reconstructed using a similar imaging mesh as the previous dataset, but in this case 250 energy bins were used over a range of 300 - 1300 keV. Again, few events are outside this range. Fig. 6 shows the simple back-projection reconstruction.

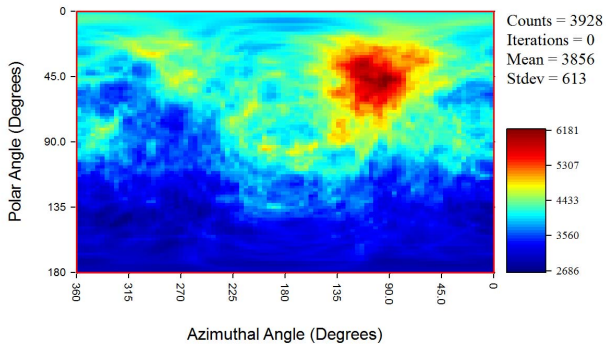

Fig. 6. The uncompensated simple back-projection reconstruction for a ^{137}Cs source moving 360° around the azimuthal direction and a stationary ^{22}Na source.

In the simple back-projection reconstruction, the direction of the stationary ^{22}Na source is obvious, whereas the moving ^{137}Cs source is less noticeable because its intensity is smeared out along the equator.

Figs. 7 - 9 show the results after 20 EM iterations of the model based algorithm. The expected results in this situation would estimate a single hotspot in the stationary backdrop with a ^{22}Na spectrum and a hotspot at 662 keV in the target object space, which tracked the ^{137}Cs source motion. The actual reconstruction for the backdrop space, seen in Fig. 7, is similar to expectations. The lower plot shows the single hotspot at the ^{22}Na energies, and even though there is again some ^{137}Cs contamination in the backdrop, it again does not form a single hotspot but is disbursed over the entire 4π space. The middle plot shows the spectrum, but it has a significant amount of ^{137}Cs contamination. Fig. 8 shows the spectrum just in the direction of the stationary ^{22}Na source, which is a well-deconvolved ^{22}Na spectrum as expected. Fig. 9 shows the reconstruction results for the target object space. The upper image shows the hotspot at the ^{137}Cs energy, and the lower plot shows that there is no cross talk at the ^{22}Na energies. The spectrum in the middle is a well deconvolved ^{137}Cs spectrum.

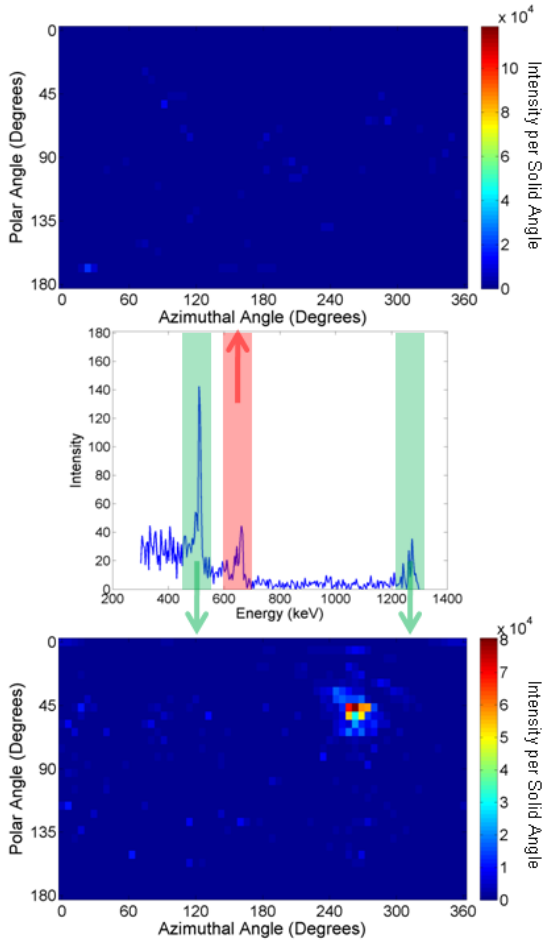

Fig. 7. Results for the backdrop space after 20 EM iterations for a moving ^{137}Cs source and a stationary ^{22}Na source. The upper plot is the deconvolved image for the pink-highlighted ^{137}Cs energy window, and the lower plot is the deconvolved image for the green-highlighted ^{22}Na energy window. The middle plot shows the deconvolved energy spectrum for the entire backdrop space.

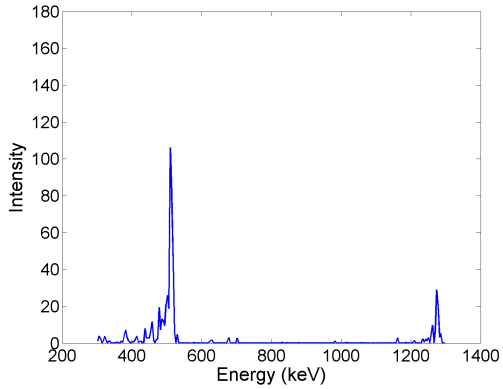

Fig. 8. The spectrum corresponding to just the hotspot direction in the lower plot of Fig. 7.

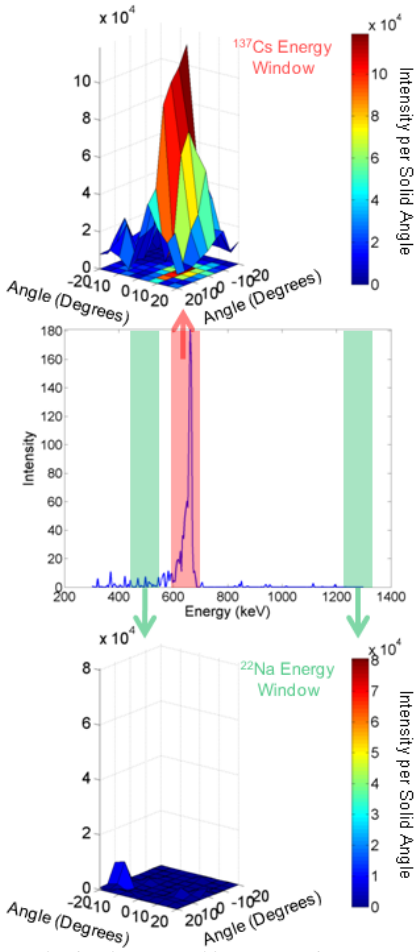

Fig. 9. Results for the target object space after 20 EM iterations for a moving ^{137}Cs source and a stationary ^{22}Na source. The upper plot is the deconvolved image for the pink-highlighted ^{137}Cs energy window, and the lower plot is the deconvolved image for the green-highlighted ^{22}Na energy window. The middle plot shows the deconvolved energy spectrum for this target.

C. Two sources moving in opposite directions

In the final experiment, a ^{137}Cs source was rotated 360° around the detector system similar to the first experiment, and then a ^{22}Na source was rotated 360° around the detector in the opposite direction. The two datasets were then combined and reconstructed as if they occurred simultaneously. This combined dataset was reconstructed using a similar imaging and energy meshes as the previous experiment (except that now there are two target object meshes tracking the two moving sources). The simple back-projection image for this dataset looks very similar to that of the first reconstruction, a smear of activity through the equator, and without tracking information, the two sources would appear to simply overlap. 4449 events were reconstructed in the energy range of 300 keV to 1300 keV.

The results for the model based algorithm after 20 EM iterations is shown in Figs. 10 & 11. The expected results for this reconstruction would be zero (or some small amount of background) in the backdrop space, and a single hotspot at the

^{137}Cs energy in the target object tracking the ^{137}Cs source, and a single hotspot at the ^{22}Na energies for the target object tracking the ^{22}Na source. The backdrop results seen in Fig. 10 show roughly the expected results. Some ^{137}Cs and ^{22}Na intensity is incorrectly estimated in the backdrop, but this contamination is small and dispersed in all directions. Fig. 11 shows the results for the two target objects. Here it is obvious that the target object tracking the ^{137}Cs source has a single hotspot at 662 keV and a zero distribution at the ^{22}Na energy window. Also, the target object tracking the ^{22}Na source has a hotspot at the ^{22}Na energies and a flat distribution at the ^{137}Cs energy as expected. Finally, the spectra for the two target objects show well deconvolved ^{137}Cs and ^{22}Na energy spectra.

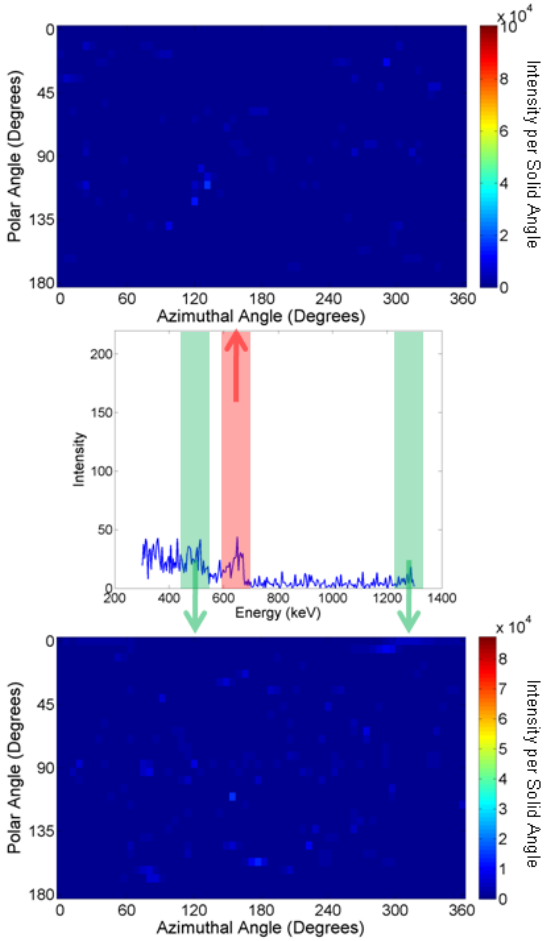

Fig. 10. Results for backdrop space after 20 EM iterations for a ^{137}Cs source moving counterclockwise and a ^{22}Na source moving clockwise. The upper plot is the deconvolved image for the pink-highlighted ^{137}Cs energy window, and the lower plot is the deconvolved image for the green-highlighted ^{22}Na energy window. The middle plot shows the deconvolved energy spectrum for the entire backdrop space.

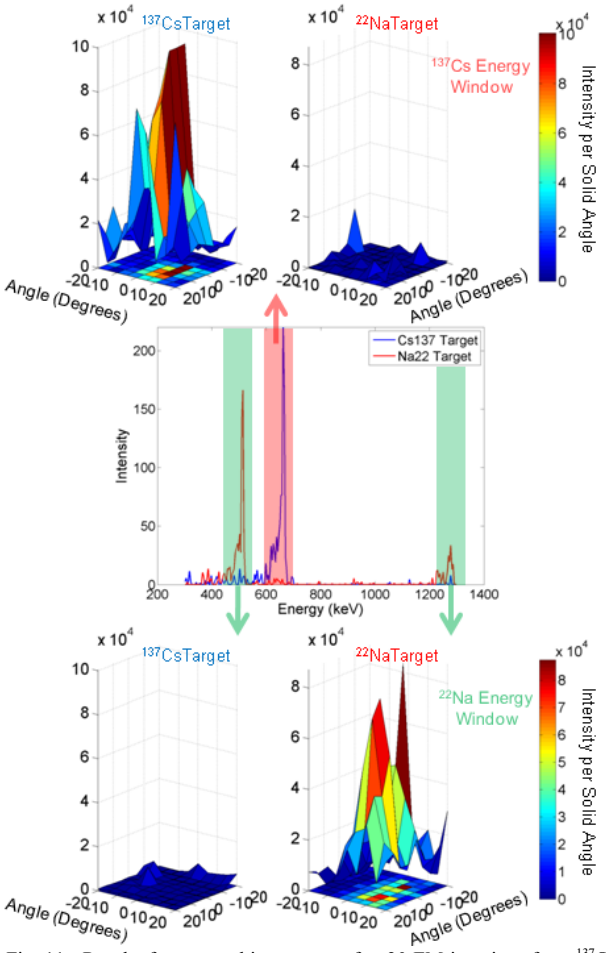

Fig. 11. Results for target object spaces after 20 EM iterations for a ^{137}Cs source moving counterclockwise and a ^{22}Na source moving clockwise. The upper plots are the deconvolved images for the pink-highlighted ^{137}Cs energy window, and the lower plots are the deconvolved images for the green-highlighted ^{22}Na energy window. The images on the left correspond to the target object space tracking the ^{137}Cs source, and those on the right correspond to the target object space tracking the ^{22}Na source. The middle plot shows the deconvolved energy spectra for the two target objects.

VI. Conclusions

A model-based reconstruction method was presented that successfully deconvolves moving source(s) with known motion from stationary sources with minimal cross-talk contamination between sources. This new approach is an extension of the standard MLEM reconstruction for the combined energy and spatial domain. Even in the case of target objects that overlap in the course of their motion, the maximum likelihood model can be used to estimate the contribution from each of the target objects. This allows the simultaneous imaging of the gamma-ray emissions from a number of simultaneously moving target objects and a non-moving backdrop as long as the motion paths are known. We have demonstrated this method using several situations and data from Polaris, an 18-detector position-sensitive CZT array system.

ACKNOWLEDGMENT

The authors would like to thank the ORION team especially Willy Kaye, Yvan Boucher, and Feng Zhang for their work on the Polaris system used for the measurements in this paper. Also, thanks to Jim Berry for his work on Polaris and assembly of the actuator positioning system.

REFERENCES

[1] D.Xu, Z. He, and F. Zhang, "Detection of gamma ray polarization using a 3-D position-sensitive CdZnTe detector," *IEEE Trans. Nucl. Sci.*, vol. 52, no. 4, pp. 1160-1164, Aug. 2005.

[2] D. Xu and Z. He, "Filtered back-projection in 4π Compton imaging with a single 3D position sensitive CdZnTe detector," *IEEE Trans. Nucl. Sci.*, vol. 53, no. 5, pp. 2787-2796, Oct. 2006.

[3] F. Zhang, Z. He, and C. E. Seifert, "A prototype three-dimensional position sensitive CdZnTe detector array," *IEEE Trans. Nucl. Sci.*, vol. 54, no. 4, pp. 843-848, Aug. 2007.

[4] T. Aucott, F. Jensen, and M. Bahr, "Machine vision radiation detection system," *In ARI Conf.*, 2009.

[5] D. Hochbaum, The multi-sensor nuclear threat detection problem, 2009, ISSN 1387-666X Volume 47 Operations Research and Cyber-Infrastructure SPriger US Part III Subpart 6 pages 389-399.

[6] B. D. Yanoff et al., "GE intelligent personal radiation locator system," *In ARI Conf.*, 2009.

[7] D. Xu, and Z. He, "Gamma-ray energy-imaging integrated spectral deconvolution," *Nucl. Inst. Meth. Phys. Res. A.,* vol. 574, no. 1, pp. 98-109, April 2007.

[8] H. H. Barrett, T. White, and L. C. Parra, "List-mode likelihood," *J. Opt. Soc. Am. A*, Vol. 14, no. 1, pp. 2914-1923, Nov. 1997.

[9] L. C. Parra and H. H. Barrett, "List-mode likelihood - EM algorithm and noise estimation demonstrated on 2D-PET," *IEEE Trans. Med. Imag.*, vol. 17, no. 2, pp. 228-235, April 1998.

[10] Y. Censor, "Finite series expansion reconstruction methods," *Proc. IEEE*, vol. 71, no. 3, pp. 409-419, March 1983.